ACS OMEGA

Open Access



http://pubs.acs.org/journal/acsodf

Article

# Development of Spiropyran Immobilization and Characterization Protocols for Reversible Photopatterning of $SiO_2$ Surfaces

Bokun Zhou, Alexander Govyadinov, Pavel Kornilovitch, and Vincent T. Remcho*

Cite This: *ACS Omega* 2024, 9, 29401−29409

Read Online

ACCESS | Metrics & More | Article Recommendations | Supporting Information

**ABSTRACT:** Spiropyran is a dynamic organic compound that is distinguished by its reversible conversion between two forms: the colorless closed spiropyran (SP) form and the purple open merocyanine (MC) form. Typically triggered by UV light and reversed by visible light, spiropyran-functionalized surfaces offer reversible conversion in properties including color, polarity, reactivity, and fluorescence, making them applicable to diverse applications in chemical sensors, biosensors, drug delivery, and heavy metal extraction. While spiropyran has been successfully incorporated into various material platforms with $SiO_2$ surfaces, its application on flat surfaces has been limited due to surface area constraints and a lack of standardized evaluation methods, which largely depend on the integration approach and substrate type used. In this study, we systematically review the existing literature and categorize integration methods and substrate types first and then report on our experimental work, in which we developed a streamlined three-step immobilization protocol, which includes surface activation, amination with (3-aminopropyl) triethoxysilane (APTES), and subsequent functionalization with carboxylic spiropyran (SP-COOH). Using $SiO_2$ surfaces as a demonstration, we have also established a robust characterization protocol, consisting of contact angle measurements, X-ray photoelectron spectroscopy (XPS), ellipsometry, and fluorometric analysis. Our results evaluate the newly developed immobilization protocol, demonstrating effective activation and optimal amination using a 2% APTES solution, achieved in 5 min at room temperature. Fluorescence imaging provided clear contrast between the SP and the MC forms. Furthermore, we discuss limitations in the surface density of functional groups and steric hindrance and propose future improvements. Our work not only underscores the versatility of spiropyran in surface patterning but also provides optimized protocols for its immobilization and characterization on $SiO_2$ surfaces, which may be adapted for use on other substrates. These advancements lay the groundwork for on-chip sensing technologies and other applications.

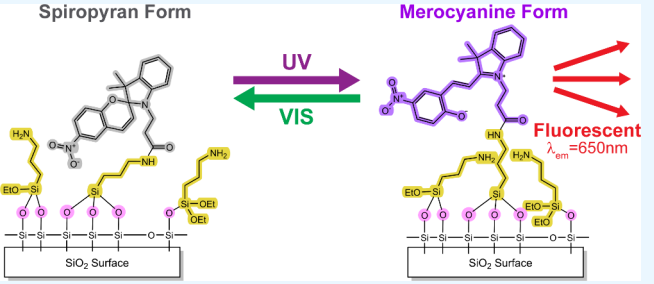


## 1. INTRODUCTION

Spiropyran and its derivatives, recognized as dynamic organic molecules, exhibit reversible conversions in response to various environmental stimuli, including light, temperature, pH, solvent polarity, metal ions, and mechanical stress.[1,2] Known for their photochromism, these compounds undergo structural isomerization from the ring-closed spiropyran (SP) to the ring-opened merocyanine (MC) forms when exposed to UV light, which could be reversed by visible light, as shown in Figure 1. Structurally, spiropyran comprises a benzopyran moiety and an indoline moiety, linked by a tetrahedral $sp^3$ spiro carbon atom (highlighted in blue). In its SP form, it adopts a compact, 3D orthogonal configuration. However, upon UV irradiation, the C−O bond breaks, leading to an expanded, 2D planar configuration as the MC form. During such isomerization, the dipole moment also changes due to the separation of charge centers, resulting in a redshift in the absorption band. As a result, the SP form is hydrophobic and colorless and the MC form is hydrophilic and purple, exhibiting enhanced intermolecular interactions and increased solubility in polar solvents. In addition, only the MC form is reported to be fluorescent, and

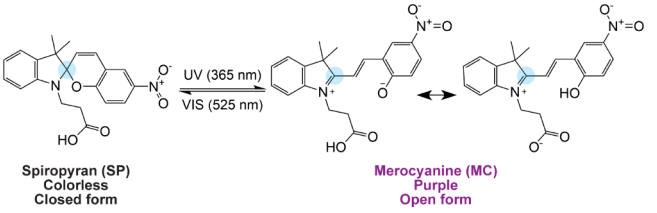


**Figure 1.** Photochromism occurs between the colorless closed spiropyran (SP) form and the purple open merocyanine (MC) form. Normal and reverse photochromism is triggered by UV light (365 nm) and visible light (525 nm), respectively. The central spiro-carbon is highlighted in blue.

**Received:** February 19, 2024
**Revised:** June 3, 2024
**Accepted:** June 7, 2024
**Published:** June 24, 2024

Table 1. Comparison of Integration Methods and Substrate Types for Addition of Spiropyrans with $SiO_2$ Surfaces

| Integration Methods | Substrate Type | Characterization Method | Purpose/Application |
|---|---|---|---|
| General sol−gel method | Silica gel | UV−vis, SEM | Effect of medium polarity,[14] additive,[15] or substituent[16] on photochromism of spiropyran-incorporated silica gel |
| | Silica thin film | UV−vis, SEM, FTIR, Ellipsometry | Photochromism of spiropyran-incorporated silica films; Mechanism and stability[17,30] |
| Physical Adsorption | Silica, mesoporous | UV−vis, SEM, FTIR | Light controlled adsorption of merocyanine;[31] Light controlled drug release[18] |
| | Silica, dendritic fibrous | UV−vis, SEM, FTIR | Light controlled adsorption of merocyanine; Effect of pore size on kinetics of photochromism[19] |
| | Silica nanoparticles | UV−vis, SEM, FTIR | Effect of spiropyran and Si molar ratio on kinetics; Dynamic anticounterfeiting[32] |
| Surface Modification with silane chemistry (APTES) | Glass slide; Silica capillary | UV−vis, WCA, Fluorescence | Light controlled change in contact angle and wetting properties; Light controlled capillary rise[25,33] |
| | Silica, colloidal films | SEM, CV | Light controlled ion transport through spiropyran-modified nanoporous films[26] |
| | Silica microbeads | UV−vis | Light controlled metal ion extraction[20] |
| | Silica, particles | UV−vis, SEM | Light controlled aggregation and dispersion of spiropyran-modified silica particles[27] |
| | Silica, mesoporous | UV−vis, SEM, FTIR, WCA | Light controlled drug delivery and release;[28] Light controlled fluoride adsorption;[21] pH gated size control for drug release[34] |
| Advanced Modification | Silicon wafer; Glass slide | UV−vis, TEM | Polymer brushes; Light controlled change in contact angle and wetting properties[29] |
| | Silica capillary | UV−vis, FTIR | Polymer brushes; Spiropyran-integrated capillary sensor[22] |
| | Silica, mesoporous | UV−vis, TGA | Silylated spiropyran; Light controlled metal ion extraction[23] |

its intensity could be improved by solvent polarity, pH, or incorporation into nanoporous frameworks.[2−4] Leveraging these versatile features, spiropyran and its derivative have been employed as chemosensors for detecting pH,[4,5] solvent polarity,[6] $CO_2$ gas,[7] $Cu^{2+}$ ions,[8] and aniline pollutants.[9] Their unique capability to distinctly respond to single or multiple stimuli positions them as ideal candidates for orthogonal sensing systems, utilizing unified colorimetric or fluorometric detection methods.[9−11]

To refine our investigation within the vast spectrum of spiropyran applications, our research specifically focuses on its integration with silicon dioxide ($SiO_2$) surfaces, chosen for their distinctive optical properties, biocompatibility, thermal stability, and straightforward surface chemistry amenable to surface functionalization.[12,13] Table 1 summarizes various integration methods and substrate types documented in the literature, highlighting the applications of spiropyran on $SiO_2$ surfaces. Early work incorporates spiropyran within silica gel matrices via sol−gel process, probing the effect of a polar environment,[14] additives,[15] and substituents[16] on photochromic behavior. It has been demonstrated that silica gel stabilizes the SP-MC equilibrium, favoring the MC form due to hydrogen bonding between the oxygen anion from the MC form and hydroxyl groups on the $SiO_2$ surface.[17] Subsequent research explored the enhanced adsorption of the MC form over the SP form onto mesoporous[18] and dendritic fibrous silica,[19] revealing how pore sizes influences kinetics and sensing capability.[20−23] Nonetheless, these applications involved only physical adsorption of spiropyran, leading to challenges with reagent loss, reproducibility, and long-term stability. For permanent integration of spiropyran onto surfaces, chemical modification of both the $SiO_2$ surface and spiropyran is essential. A prevalent method is the use of silane chemistry to attach amine groups to the surface, which can react with spiropyran molecules that have been functionalized with hydroxyl,[24] carboxyl,[20,25] or other reactive groups.[24,26−28] Moreover, advanced modification techniques have improved the integration of spiropyran into silica-based materials. Spiropyrans have been embedded as pendant groups within monomers, such as methyl methacrylate[29] or norbornene,[22] which are then polymerized onto modified $SiO_2$ surfaces. Silylation of spiropyran[23] is an alternative approach, allowing for co-condensation with the silanol groups on the $SiO_2$ surface.

The selection of the characterization methods largely depends on the type of substrate being analyzed. As summarized in Table 1, UV−vis spectroscopy is widely applicable to a range of substrates, including solutions, sol−gel matrices, and flat surfaces. It effectively distinguishes between the SP and MC forms of spiropyran and assesses their conversion kinetics. Ellipsometry, ideal for thin film applications, assists in verifying the presence of spiropyran by measuring changes in the refractive index and thickness. Similarly, scanning electron microscopy (SEM) provides qualitative images that showcase morphological changes. Fourier transform infrared spectroscopy (FTIR) is adept at detecting spiropyran by identifying shifts in the intensities of peaks characteristic of spiropyran versus those of the substrate. However, distinguishing between the SP and MC forms remains challenging with FTIR due to the complexity in the fingerprint region. Water contact angle (WCA) measurement is effective with flat surfaces and can measure the contrast between the SP and MC forms. However, it is limited by the coverage of spiropyran and surface energy, which can also be affected by the substrate. Fluorometric analysis is useful with both solution and solid phases, exploiting the nonfluorescent nature of the SP form and the weak fluorescence of the MC form. One of the primary challenges in comparative analysis across different materials platforms is the diversity of integration methods, substrate types, and characterization methods. Streamlined and optimized protocols of immobilization and characterization are therefore of importance for easy and universal assessment.

In this work, we developed a streamlined three-step immobilization protocol tailored for $SiO_2$ surfaces. This protocol encompasses activation, amination, and functionaliza-


https://doi.org/10.1021/acsomega.4c01607
ACS Omega 2024, 9, 29401−29409

tion steps. Due to the well-defined surface and interface of $SiO_2$, we employed a suite of characterization techniques to evaluate and optimize the immobilization protocol. These techniques include contact angle measurement, X-ray photoelectron spectroscopy (XPS), ellipsometry, and fluorometric analysis. We determined that activation with a piranha solution is effective. By optimizing the reaction time, temperature, and concentration, we successfully achieved a thin and uniform layer of APTES. Fluorometric analysis further confirmed the distinct contrast between the SP and the MC forms. Our work demonstrates the efficacy of streamlined and optimized protocols for immobilization and characterization, which could be adapted to other materials platforms, aiming for broader applications. In the end, we discuss the limitations of our current approach and propose future research directions to build upon these findings.

## 2. MATERIALS AND METHODS

**2.1. Activation with Oxygen Plasma, HCl, and Piranha Solution.** Silicon wafers with a 200 nm thermally grown $SiO_2$ layer, diced into 1" × 1" coupons, were obtained from HP Inc. (Corvallis, OR). They were used as flat, rigid substrates. The initial $SiO_2$ thickness was determined using ellipsometry (Film Sense FS-1 Multiwavelength Mapping Ellipsometer), employing 9-point mapping to ensure uniformity. The variation in thickness was confirmed to be less than 0.3 nm. The coupons were rinsed with deionized water (DIW), followed by nitrogen blow-drying, and stored in a covered chip tray (Stat-Pro 150, 3 × 3) to avoid contamination. For comparison, Whatman glass microfiber discs (GE Healthcare Bio Sciences, Pittsburgh, PA) were used as porous flexible substrates.

Three surface activation methods were employed: oxygen plasma treatment, hydrochloric acid (HCl), and piranha solution. Oxygen plasma treatments were conducted at an RF power of 15W and a pressure of 0.6 Torr for 5 min using an Evactron RF plasma cleaner (Redwood City, CA) in a custom vacuum chamber. Acid treatment included immersing the coupons in 0.1 M NaOH for 5 min, rinsing with DIW, and then immersing in 1 M HCl for another 5 min. Piranha solution was prepared by slowly adding 10 mL of 30% $H_2O_2$ into 30 mL of concentrated $H_2SO_4$ (v:v = 1:3) and allowed to cool for 5 min. The pretreated coupons were then immersed in this solution for 15 min, with occasional stirring. Following treatment, the coupons were rinsed with DIW and dried using nitrogen blow-drying.

**2.2. Amination with APTES.** (3-Aminopropyl) triethoxysilane (APTES, CAS No. 919−30−2) was purchased from Sigma-Aldrich (St. Louis, MO). To prepare various concentrations of the APTES solution, for example, a 2% APTES solution was made by adding 1 mL of APTES to 49 mL of ethanol, keeping the total volume at 50 mL. The solution was thoroughly mixed and then transferred to a covered Petri dish to minimize evaporation during heating. The dish was subsequently placed on a hot plate, with the temperature regularly monitored until the desired level was reached.

Following the activation step, the coupons were immediately immersed in the APTES solution for predetermined durations. After immersion, the coupons were removed from the solution and rinsed with ethanol to remove any unbound APTES. For more thorough cleaning, sonication in ethanol was employed for 5 min to effectively remove loosely adhered APTES. Following nitrogen blow-drying, the coupons were placed in an oven set at 115 °C for 5 min to facilitate further condensation of the APTES layer on the $SiO_2$ surface.

**2.3. Functionalization with SP-COOH.** Carboxylic spiropyran (SP-COOH), specifically 3-(3′,3′-dimethyl-6-nitrospiro[chromene-2,2′-indole]-1′-yl) propanoic acid (CAS No. 55779−26−5), was obtained from BioChemPartner (Shanghai, China). The chemical structure of SP-COOH was verified via 1H NMR, with data provided by the BioChemPartner. The excitation and emission wavelengths characteristic of carboxylic spiropyran were identified in the solution phase (ethanol solution) as 585 and 630 nm, respectively. A spiropyran solution was prepared by dissolving 40 mg of SP-COOH in ethanol. Given the purity of our sample, it was then filtered through a PTFE filter (0.1 $\mu$m) before being transferred to a Petri dish.

Subsequently, 40 mg of *N*-(3-(dimethylamino)propyl)-*N*′-ethyl carbodiimide hydrochloride (EDC, CAS No. 25952−53−8) from Sigma-Aldrich was added to the filtered solution to reach a total volume of 40 mL. The Petri dish with cover was placed on a shaker and stirred for 30 min to ensure thorough mixing. Aminated coupons were then immersed into the solution and incubated for 18 h to allow for the functionalization process, while kept in the dark.

Following incubation, samples were rinsed first with ethanol and then with DIW. To ensure the complete removal of any loosely bound residues, sonication could also be performed as an additional cleaning step. The samples were then dried by using nitrogen blow-drying.

**2.4. Characterization Setup.** Contact angle measurements were performed using a home-built setup with a camera focused on the cross-section of the substrate. A 5-$\mu$L droplet of DIW was dispensed vertically onto the sample surface using an automatic pipet, and images were captured immediately thereafter. Contact angles were analyzed using ImageJ software (National Institutes of Health, USA), with data collected in triplicate and averaged. Due to the accuracy of this setup, contact angles are reported as a range.

Ellipsometry measurements employed an automated 9-point mapping setting. The ellipsometry model used a standard $SiO_2$/Si model, comprising a silicon layer and a silicon dioxide layer, assuming uniformity without any interfacial layer or surface roughness. Averaged thickness along with relative variation, is reported. Postamination, similar measurements on the same samples indicated that the relatively thin APTES growth (less than 10 nm) compared to the thicker $SiO_2$ layer did not significantly affect the overall refractive index. Thus, in our model, the presence of APTES was assumed to predominantly impact the layer thickness rather than the refractive index of the $SiO_2$ layer. Due to the accuracy of this setup, thickness variation below 0.2 nm is close to the margin of error and is excluded from discussion.

X-ray photoelectron spectroscopy (XPS) analysis was conducted in collaboration with HP Inc., focused on elemental composition and chemical states on the sample surface. Utilizing a monochromatic Al K$\alpha$ X-ray source, high-resolution scans targeted key elements, such as silicon, oxygen, nitrogen, and carbon. Analysis of surface atomic concentrations is conducted for the modified surfaces.

Fluorescence microscopy was performed using a Zeiss Axio Imager Microscope with an excitation filter centered at 568 nm (Chroma, S568/24X) and an emission filter centered at 655 nm (Chroma, D655/40M). Fluorescence illumination was provided by an X-Cite Series 120 fluorescence lamp. Spiropyran-


https://doi.org/10.1021/acsomega.4c01607
ACS Omega 2024, 9, 29401−29409

**Scheme 1. Schematic Representation of the Spiropyran Immobilization Protocol on $SiO_2$ Substrates**[a]

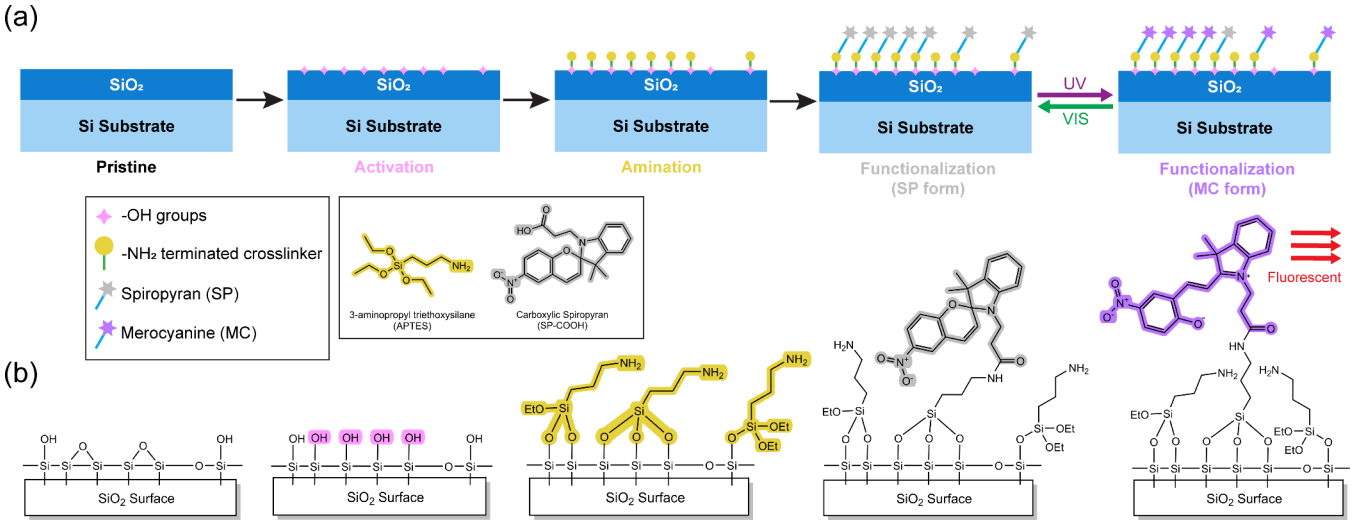


[a](a) The sequential steps of surface activation, amination, and functionalization are depicted, leading to the reversible conversion between the SP and MC forms upon UV/VIS irradiation. (b) The surface chemistry evolution is illustrated at each stage, highlighting the introduction of −OH groups during activation, attachment of $-NH_2$ terminated APTES during amination, and SP-COOH functionalization. The final panel shows the fluorescent MC form for characterization.

immobilized samples were treated with UV light at 365 nm (VWR UV Hand Lamps 365 nm/254 nm UV, 6-W). Images were analyzed using ImageJ to extract and evaluate RGB channel signals, allowing for the observation of fluorescence changes between the SP and MC forms and thus demonstrating the efficacy of spiropyran functionalization on the surface.

Scheme 1 offers a visual summary of the spiropyran immobilization process on $SiO_2$ substrates. Part (a) depicts the generalized sequence of steps: surface activation, amination, and functionalization, leading to the reversible conversion between the SP and MC forms upon UV/vis light exposure. Part (b) details the specific surface chemistry changes involved in this study, including the introduction of −OH groups during activation, attachment of $-NH_2$ terminated APTES during amination, and SP-COOH functionalization. The final panel underscores the fluorometric analysis, capturing the fluorescent MC state upon excitation. In this paper, spiropyran and merocyanine are terms used interchangeably to denote the compound in general, whereas the SP form and MC form specifically refer to the distinct structural states of the compound.

## 3. RESULTS AND DISCUSSION

**3.1. Effectiveness of the Activation Step.** We compared three surface activation methods for their effectiveness in cleaning and activating the $SiO_2$ surface. Oxygen plasma treatment, a common method for substrate cleaning, is well-known for its effective removal of organic impurities and modification of surface chemistry by introducing hydroxyl or carboxyl groups,[35] increasing surface energy and hydrophilicity. The use of NaOH and HCl for $SiO_2$ surface treatment is inspired by chromatography and capillary electrophoresis practices, where they are routinely used to clean and maintain the surface properties of silica capillaries, resulting in a clean surface with controlled surface chemistry.[36] Similarly, piranha solution removes most organic impurities and hydroxylates most surfaces due to its strong oxidizing properties.[37]

**Table 2. Contact Angle and Surface Chemical Composition for Pristine, Activated, and Aminated Surfaces**

| Sample Surfaces | C 1s | O 1s | Si 2p | N 1s | Contact Angle |
|---|---|---|---|---|---|
| Pristine | 2.8% | 67.1% | 30.1% | - | 60°−70° |
| Activated with $O_2$plasma | 3.8% | 67.5% | 28.8% | - | 10°−15° |
| Activated with NaOH and HCl | 2.8% | 67.6% | 29.6% | - | 10°−15° |
| Activated with $H_2SO_4$ | 2.7% | 67.6% | 29.7% | - | 10°−15° |
| Aminated with 2% APTES 5 min @ 20 °C | 22.4% | 50.7% | 24.1% | 2.8% | 30°−40° |
| Aminated with 2%APTES 10 min @ 20 °C | 40% | 36.9% | 18.0% | 5.1% | 30°−40° |

To evaluate the effectiveness of these methods, XPS and contact angle measurements were utilized, with the results detailed in Table 2. A pristine $SiO_2$ surface, being slightly hydrophilic, typically exhibits a contact angle of 60°−70°. Postactivation, a decrease in the contact angle indicative of increased surface energy was observed. XPS analysis revealed only C, O and Si atoms are present on the surface and no significant differences in surface composition among the activation methods. However, surfaces treated with oxygen plasma showed marginally higher carbon content, possibly due to the instrument's previous use on different surfaces, leading to carbon contamination—a common issue with shared oxygen plasma instruments. In contrast, wet treatments yielded more consistent results. Based on these findings, piranha solution treatment was selected for future experiments. Overall, the surface was effectively cleaned and activated for subsequent experimental steps.

**3.2. Thin-Layer Growth of APTES in the Amination Step.** Post activation, APTES deposition onto $SiO_2$ surfaces was achieved by immersion in APTES/ethanol solutions. Previous studies have indicated challenges with APTES growth, such as self-cross-linking, physisorption and suboptimal orientation,[38,39]



https://doi.org/10.1021/acsomega.4c01607
ACS Omega 2024, 9, 29401−29409

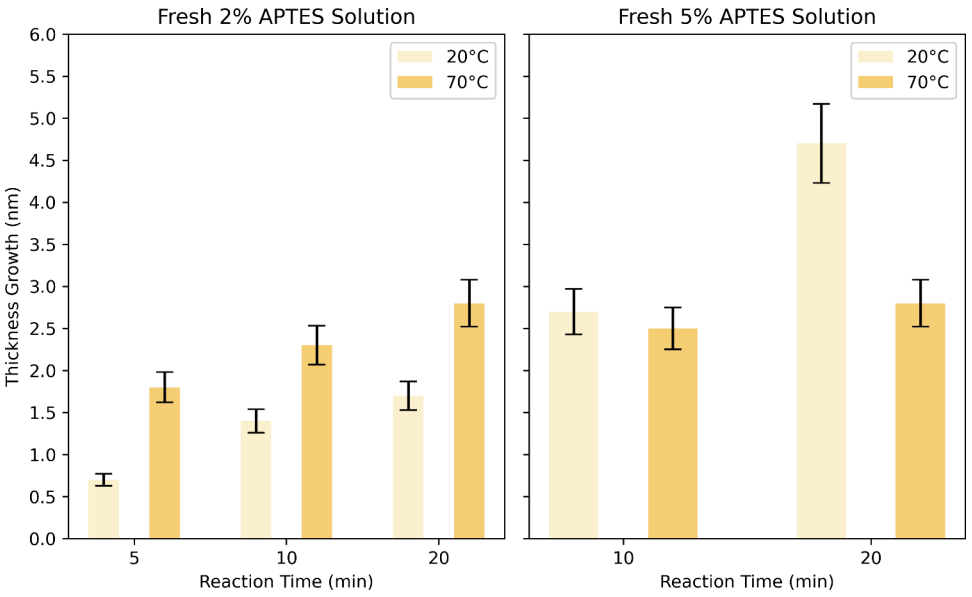


**Figure 2.** Effect of reaction conditions on the growth of APTES layers. (a) With a 2% APTES solution, a decrease in reaction time and temperature correlates with a thinner APTES layer formation. (b) With a 5% APTES solution, the layer thickness growth is less sensitive to changes in reaction time and temperature, exhibiting a less pronounced trend.

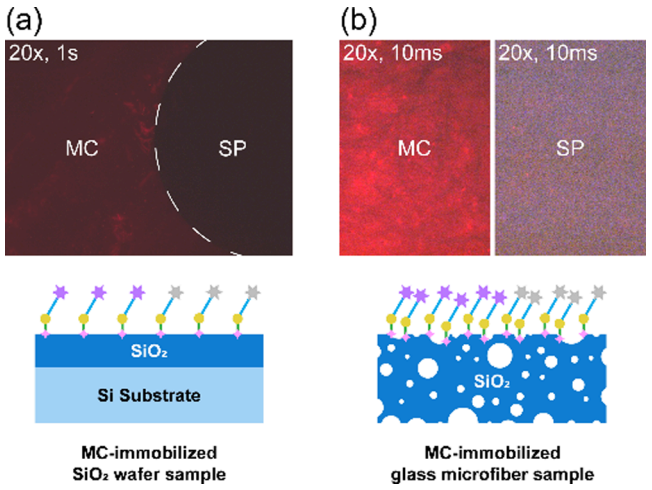


**Figure 3.** Comparative fluorescence imaging of MC-immobilized surfaces. (a) Contrast on a flat, rigid $SiO_2$ wafer substrate between areas where spiropyran is predominantly in the MC form (left) and areas in the SP form (right). (b) Contrast on a porous, flexible glass microfiber substrate between areas where spiropyran is predominantly in the MC form (left) and areas in the SP form (right). All images were captured at 20× magnification with adjusted exposure times to prevent overexposure. The illustrations below each image depict the corresponding substrate type, highlighting the difference in the surface morphology.

which could lead to a reduction in available amine groups for subsequent functionalization. To attain uniform and effective APTES coverage, an ideal scenario would be a monolayer with $-NH_2$ groups oriented outward from the substrate.

We tuned the growth of the APTES layer by adjusting the reaction conditions, including the APTES concentration, reaction time, and temperature. Ellipsometry was employed to estimate the APTES thickness; we determined the change in $SiO_2$ layer thickness pre- and postamination, attributing any increase to APTES presence. Freshly prepared APTES solutions were crucial, as aged solutions could lead to APTES aggregation, inconsistent thickness growth from batch to batch, and poor reproducibility.

As demonstrated in Figure 2, the APTES concentration plays a pivotal factor. For the 2% APTES solution, reduction in the reaction time and temperature resulted in thinner layer growth. By comparison, 5% APTES solution resulted in less consistent thickness changes, showing no discernible pattern relative to reaction temperature and time. Although further reduction in APTES concentration was possible, it led to less reproducible results. Additionally, our ellipsometry setup could detect changes with sensitivity around 0.2 nm. Based on Figure 2a, we concluded that a 2% APTES solution at room temperature for 5 min led to a thin-layer growth of 0.7 nm, indicative of good uniformity. This thin-layer approach prevents the $-NH_2$ groups from being buried inside a bulk layer. It was further validated using fluorescein isothiocyanate (FITC) as a fluorescent marker, which labels $-NH_2$ on the aminated $SiO_2$ surface. Samples treated to generate a thin-layer, a thick-layer or no-layer (control) of APTES were incubated with FITC solution. The green fluorescence intensity measured for each of these samples showed stronger signals for samples with thin layers of APTES, indicating that more $-NH_2$ is available for labeling on the surface (see Supporting Information).

XPS analysis was also conducted on the aminated surfaces, as summarized in Table 2. Compared with pristine and activated surfaces, the detection of nitrogen atoms confirmed the presence of APTES on the aminated surface. By separating silicon signals from organic and inorganic sources, we deduced the organosilicon content that came from the APTES layer. For a 2% APTES solution incubated at room temperature, we observed organosilicon percentages of 2.7% for a 5 min sample and 4.7% for 10 min sample. This data indicates that a 5 min incubation period is sufficient for forming an APTES layer ($C_9H_{23}NO_3Si$, N:Si = 1:1) without significant self-polymerization or structural issues, as evidenced by the near-equal ratio of nitrogen to organosilicon (2.8% vs 2.7%).


https://doi.org/10.1021/acsomega.4c01607
ACS Omega 2024, 9, 29401−29409

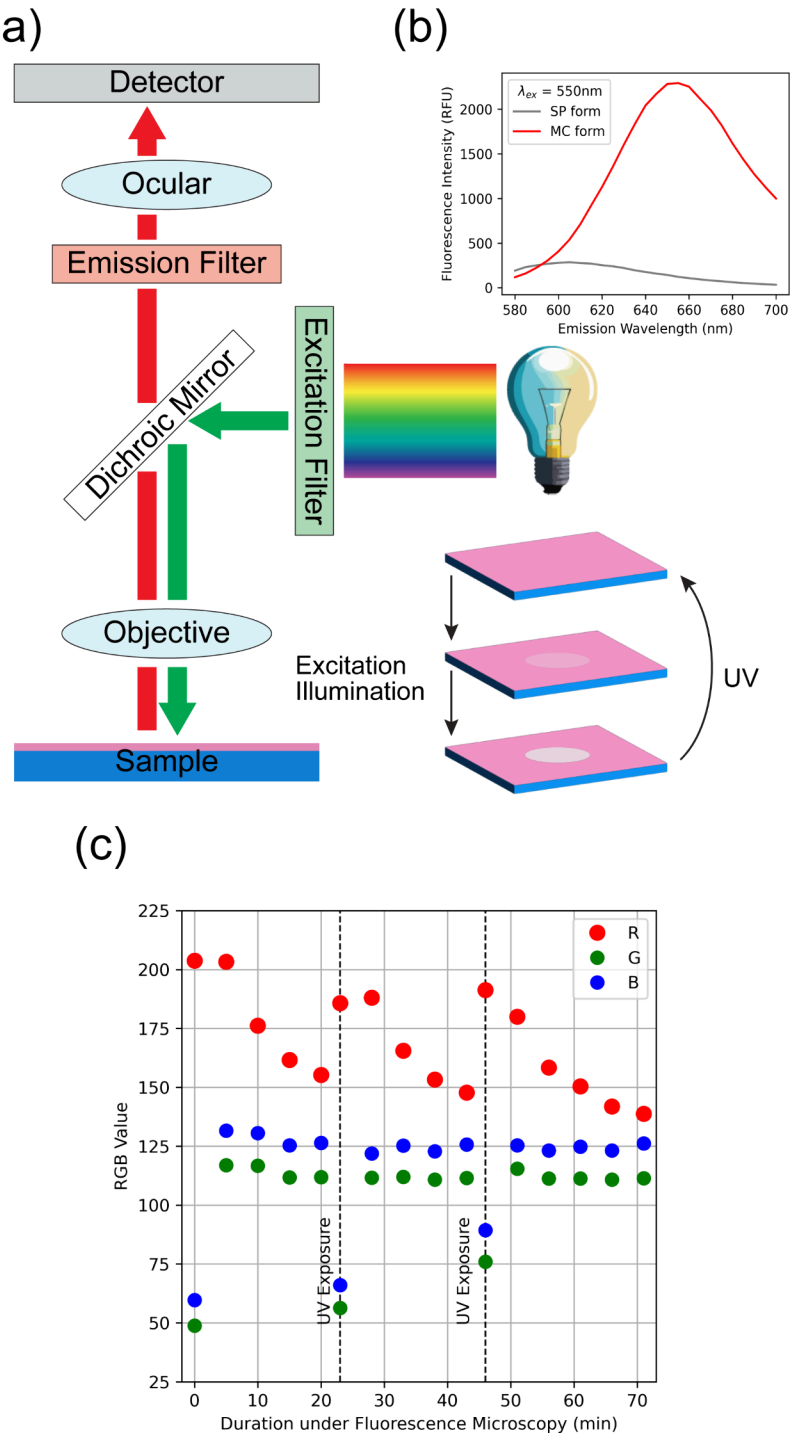


**Figure 4.** (a) Fluorescence microscopy setup utilizing excitation and emission filters to measure the red fluorescence from the spiropyran-immobilized samples. The inset displays the change in the observed area (circle) over time during fluorescence measurement, which is attributed to the MC-to-SP conversion. (b) Fluorescence spectra of samples with spiropyran-immobilized surface, showing clear contrast of red fluorescence between SP and MC forms, excited at 550 nm. (c) RGB analysis from fluorescence microscopy of spiropyran-immobilized glass microfiber surfaces over time. The RGB values, extracted from a series of images taken at 20× magnification with 10 ms exposure. The red channel (R) shows a decreasing trend due to the photochromic conversion of MC to SP, while the initial red fluorescence signals the presence of the fluorescent MC form. Periodic UV exposure demonstrates the reversibility of the process, momentarily intensifying the red fluorescence signal as MC is regenerated.

In summary, careful control of the amination parameters enabled us to achieve an optimal APTES coating that was conducive to further modification.

**3.3. Reversible Fluorescence of Spiropyran-Immobilized Surfaces in the Functionalization Step.** In this step, surfaces aminated with APTES were further modified through immersion in an SP-COOH solution. Postincubation, the samples underwent a thorough rinse and drying process prior to fluorescence imaging. A 5 min UV irradiation for 5 min converted the spiropyran into the MC form. To minimize the influence of ambient light, imaging was conducted in a dark



https://doi.org/10.1021/acsomega.4c01607
ACS Omega 2024, 9, 29401−29409

room. As a result, the fluorescence image in Figure 3a shows a clear contrast between SP and MC regions.

During fluorescence microscopy, two competing mechanisms were observed and are illustrated in Figure 4a. First, the MC form exhibits red fluorescence (emission filter, 635 nm to 675 nm) upon fluorescence illumination through the excitation filter (556 nm to 580 nm). Concurrently, illumination also led to MC-to-SP conversion, diminishing the red fluorescence signal, as shown in the inset of Figure 4a. Nevertheless, areas outside the measurement field remained in the MC form. By selectively focusing on a single area for an extended period and then quickly shifting to an adjacent area, we captured the distinct contrast between the MC and SP forms, as depicted in Figure 3a. Area on the right turned into the SP form due to the extended period of illumination. The boundary between the illuminated and nonilluminated areas is marked by the dashed white line.

However, this contrast was less discernible to the naked eye due to the relatively low fluorescence yield.[1,2] To further elucidate the fluorescence behavior of merocyanine on the $SiO_2$ surface, parallel experiments on glass microfiber paper were performed. Following activation with HCl acid, amination with 2% APTES at room temperature for 5 min, and functionalization with SP-COOH, an increase in fluorescence was noted, shown in Figure 3b. The exposure times were adjusted to avoid overexposure while ensuring discernible contrast between the SP and MC forms.

Both substrates share identical $SiO_2$ surface chemistry and underwent the same immobilization protocols: silicon wafer with a thermally grown $SiO_2$ layer in Figure 3a and glass microfiber filter paper in Figure 3b. Their main differences are that silicon wafer serves as a flat and rigid example with a surface area equivalent to its projected area, whereas glass microfiber filter paper, characterized as porous and flexible, possessing a significantly larger surface area due to its porosity. This increased fluorescence is likely attributable to the larger surface area of the glass microfiber substrate, which provides more activation sites and, consequently, a greater amount of merocyanine, leading to a stronger signal.

Further RGB analysis of a series of fluorescence images, taken under continuous excitation illumination, demonstrated the decrease in red fluorescence due to reverse photochromism, shown in Figure 4c . Exposure to the UV light uniformly reverted the surface to the MC form, allowing the process to be repeated for observation.

Successful immobilization of spiropyran on flat or porous $SiO_2$ surfaces was validated by the observed red fluorescence emission of the MC form, substantiating the utility of spiropyran-functionalized surfaces in a variety of potential application areas.

**3.4. Limitations and Future Improvements.** During this study, we encountered several factors that place limits on the functionality of the spiropyran-immobilized $SiO_2$ surfaces. First, it has been reported that the surface density of −OH groups on silicate surface a physicochemical constant for a fully hydroxylated surface.[40,41] This density acts as an intrinsic limiting factor in our material platform, determining the maximum amount of merocyanine that can be accommodated on the surface. Given the low quantum yield of merocyanine, this constraint results in only modest levels of fluorescence.

Moreover, steric hindrance plays a significant role in the conversion dynamics between SP and MC forms. The MC form, in its relaxed state, occupies more space, which may hinder adjacent SP molecules from converting to MC. Furthermore, static interactions promoting MC aggregation[42,43] could inhibit their transition back to SP. Consequently, light irradiation might not efficiently convert all molecules from one form to another.

To circumvent these issues, employing porous substrates or nanoparticles to increase surface area has proven to be effective, as evidenced by our use of glass microfiber substrates. However, the benefit of increased molecular loading must be balanced against steric hindrance, which may set a limit on signal enhancement. Identifying this balance to optimize fluorescence is a promising direction for subsequent research.

Additionally, while the behavior of immobilized spiropyran is primarily governed by the surface chemistry of its aminated backbone,[1] the investigation into solvatochromism during specific applications emerges as a practical concern. Optimizing this aspect is crucial to control or eliminate undesired responses to stimuli, ensuring the system's efficacy and applicability.

Furthermore, chemical modifications targeting the phenolic −OH group of the MC form could stabilize it, prevent reverse photochromism, and preserve fluorescence. Future work will include both solution phase and surface studies aiming to refine spiropyran-functionalized surfaces.

## 4. CONCLUSION

This study developed a streamlined three-step protocol for immobilizing spiropyrans on $SiO_2$ surfaces encompassing activation, amination, and functionalization. Various characterization methods, such as contact angle measurements, XPS, ellipsometry, and fluorometric analysis, were employed to evaluate the effectiveness of the protocol. Comparisons of different activation methods indicated equivalent effectiveness. In the amination step, optimal conditions were established as 2% APTES in ethanol at room temperature for 5 min, leading to a uniform thin-layer ideal for subsequent modification. Carboxylic spiropyran was successfully immobilized using EDC click chemistry, and fluorometric analysis revealed a clear, reversible contrast between the SP and MC forms. These streamlined and optimized protocols of immobilization and characterization are potentially adaptable to other material platforms, offering a versatile foundation for future investigations. Furthermore, the limitation of current setup could be overcome by using porous substrates to increase the number of immobilized spiropyran molecules and exploring further modifications with chemicals reactive to the phenolic −OH group on the MC form. These enhancements aim to increase MC presence on surfaces, potentially extending this method for applications in on-chip sensing and microfluidic applications.

## ■ ASSOCIATED CONTENT

### Supporting Information

The Supporting Information is available free of charge at https://pubs.acs.org/doi/10.1021/acsomega.4c01607.

Fluorescence labeling of aminated $SiO_2$ surfaces for verification of the availability of amine groups; schematic of the spiropyran immobilization protocol (PDF)

## ■ AUTHOR INFORMATION

### Corresponding Author

**Vincent T. Remcho** − *Department of Chemistry, College of Science and Materials Science Program, College of Engineering, Oregon State University, Corvallis, Oregon 97331, United States;* orcid.org/0000-0002-9188-6438; Email: vince.remcho@oregonstate.edu



https://doi.org/10.1021/acsomega.4c01607
ACS Omega 2024, 9, 29401−29409

### Authors

**Bokun Zhou** − *Department of Chemistry, College of Science and Materials Science Program, College of Engineering, Oregon State University, Corvallis, Oregon 97331, United States;* orcid.org/0000-0002-4455-3876

**Alexander Govyadinov** − *HP Inc., Corvallis, Oregon 97330, United States*

**Pavel Kornilovitch** − *HP Inc., Corvallis, Oregon 97330, United States*

Complete contact information is available at: https://pubs.acs.org/10.1021/acsomega.4c01607


### Author Contributions

B. Zhou was responsible for data curation, formal analysis, methodology, investigation, validation, visualization, and writing the original draft of the manuscript. A. Govyadinov and P. Kornilovitch contributed to the conceptualization, formal analysis, project administration, and resource allocation, as well as providing supervision and participating in the review and editing of the manuscript. V. T. Remcho was involved in the conceptualization, formal analysis, funding acquisition, methodology, project administration, and resource allocation. He also provided supervision and contributed to the writing, specifically in the review and editing phases. All authors have given approval to the final version of the manuscript.

### Notes

The authors declare no competing financial interest.

## ■ ACKNOWLEDGMENTS

The authors acknowledge the financial support of the HP-OSU Seed Grant [VC2570], which included an HP-funded follow-on effort. We extend special thanks also to Dr. William Stickle for his assistance in collecting and analyzing XPS data. Furthermore, we are grateful to the members of the Remcho Research Group for their discussion and input on the editing of this manuscript.

## ■ ABBREVIATIONS

APTES, 3-aminopropyl triethoxysilane; CV, cyclic voltammetry; EDC, *N*-(3-dimethylaminopropyl)-*N*′-ethyl carbodiimide hydrochloride; FITC, fluorescein isothiocyanate; FTIR, Fourier transform infrared spectroscopy; MC form, the ring-opened form of spiropyran; SEM, scanning electron microscopy; SP form, the ring-closed form of spiropyran; SP-COOH, carboxylic spiropyran, 3-(3′,3′-dimethyl-6-nitrospiro[chromene-2,2′-indole]-1′-yl) propanoic acid; TEM, transmission electron microscopy; TGA, thermogravimetric analysis; WCA, water contact angle measurement; XPS, X-ray photoelectron spectroscopy

## ■ REFERENCES


(1) Klajn, R. Spiropyran-Based Dynamic Materials. *Chem. Soc. Rev.* **2014**, *43* (1), 148−184.

(2) Kortekaas, L.; Browne, W. R. The Evolution of Spiropyran: Fundamentals and Progress of an Extraordinarily Versatile Photochrome. *Chem. Soc. Rev.* **2019**, *48* (12), 3406−3424.

(3) Kundu, P. K.; Olsen, G. L.; Kiss, V.; Klajn, R. Nanoporous Frameworks Exhibiting Multiple Stimuli Responsiveness. *Nat. Commun.* **2014**, *5* (1), 3588.

(4) Babazadeh-Mamaqani, M.; Roghani-Mamaqani, H.; Abdollahi, A.; Salami-Kalajahi, M. Optical Chemosensors Based on Spiropyran-Doped Polymer Nanoparticles for Sensing Ph of Aqueous Media. *Langmuir* **2022**, *38* (30), 9410−9420.

(5) Babazadeh-Mamaqani, M.; Roghani-Mamaqani, H.; Abdollahi, A.; Salami-Kalajahi, M. Development of Optical Chemosensors Based on Photochromic Polymer Nanocarriers. *New J. Chem.* **2022**, *46* (31), 15080−15094.

(6) Abdollahi, A.; Alinejad, Z.; Mahdavian, A. R. Facile and Fast Photosensing of Polarity by Stimuli-Responsive Materials Based on Spiropyran for Reusable Sensors: A Physico-Chemical Study on the Interactions. *J. Mater. Chem. C* **2017**, *5* (26), 6588−6600.

(7) Shang, J.; Lin, S.; Theato, P. Fabrication of Color Changeable $CO_2$ Sensitive Nanofibers. *Polym. Chem.* **2017**, *8* (48), 7446−7451.

(8) Trevino, K. M.; Tautges, B. K.; Kapre, R.; Franco, F. C., Jr; Or, V. W.; Balmond, E. I.; Shaw, J. T.; Garcia, J.; Louie, A. Y. Highly Sensitive and Selective Spiropyran-Based Sensor for Copper(II) Quantification. *ACS Omega* **2021**, *6* (16), 10776−10789.

(9) Tian, W.; Xue, Y.; Tian, J.; Gong, P.; Dai, J.; Wang, X.; Zhu, Z. Colorimetric and Fluorometric Dual-Mode Detection of Aniline Pollutants Based on Spiropyran Derivatives. *RSC Adv.* **2016**, *6* (86), 83312−83320.

(10) Sheng, J.; Perego, J.; Bracco, S.; Cieciórski, P.; Danowski, W.; Comotti, A.; Feringa, B. L. Orthogonal Photoswitching in a Porous Organic Framework. *Angew. Chem., Int. Ed.* **2024**, *63*, No. e202404878.

(11) Dowds, M.; Stenspil, S. G.; De Souza, J. H.; Laursen, B. W.; Cacciarini, M.; Nielsen, M. B. Orthogonal- and Path-Dependent Photo/Acidoswitching in an Eight-State Dihydroazulene-Spiropyran Dyad. *ChemPhotoChem.* **2022**, *6* (10), No. e202200152.

(12) Kankala, R. K.; Han, Y.; Na, J.; Lee, C.; Sun, Z.; Wang, S.; Kimura, T.; Ok, Y. S.; Yamauchi, Y.; Chen, A.; Wu, K. C. -W. Nanoarchitectured Structure and Surface Biofunctionality of Mesoporous Silica Nanoparticles. *Adv. Mater.* **2020**, *32* (23), No. 1907035.

(13) Wang, Y.; Gou, K.; Guo, X.; Ke, J.; Li, S.; Li, H. Advances in Regulating Physicochemical Properties of Mesoporous Silica Nanocarriers to Overcome Biological Barriers. *Acta Biomater.* **2021**, *123*, 72−92.

(14) Evans, T. R.; Toth, A. F.; Leermakers, P. A. Medium Effects of Photochromism. Reversible Photobleaching of a Spiropyran on Silica Gel. *J. Am. Chem. Soc.* **1967**, *89* (19), 5060−5061.

(15) Tagaya, H.; Nagaoka, T.; Kuwahara, T.; Karasu, M.; Kadokawa, J.; Chiba, K. Preparation and Photochromism of Sulfonated Spiropyran-Silica Nanocomposites. *Microporous Mesoporous Mater.* **1998**, *21* (4−6), 395−402.

(16) Léaustic, A.; Dupont, A.; Yu, P.; Clément, R. Photochromism of Cationic Spiropyran-Doped Silica Gels. *New J. Chem.* **2001**, *25* (10), 1297−1301.

(17) Kinashi, K.; Nakamura, S.; Imamura, M.; Ishida, K.; Ueda, Y. The Mechanism for Negative Photochromism of Spiropyran in Silica. *J. Phys. Org. Chem.* **2012**, *25* (6), 462−466.

(18) Han, R.; Wu, S.; Tang, K.; Hou, Y. Facilitating Drug Release in Mesoporous Silica Coated Upconversion Nanoparticles by Photoacid Assistance upon Near-Infrared Irradiation. *Adv. Powder Technol.* **2020**, *31* (9), 3860−3866.

(19) Yamaguchi, T.; Maity, A.; Polshettiwar, V.; Ogawa, M. Photochromism of a Spiropyran in the Presence of a Dendritic Fibrous Nanosilica; Simultaneous Photochemical Reaction and Adsorption. *J. Phys. Chem. A* **2017**, *121* (42), 8080−8085.

(20) Scarmagnani, S.; Slater, C.; Lopez, F. B.; Diamond, D.; Walsh, Z.; Paull, B.; Macka, M. Photoreversible Ion-Binding Using Spiropyran Modified Silica Microbeads. *Int. J. Nanomanufacturing* **2010**, *5* (1/2), 38.

(21) Guan, X.; He, M.; Chang, J.; Wang, Z.; Chen, Z.; Fan, H. Photo-Controllability of Fluoride Remediation by Spiropyran-Functionalized Mesoporous Silica Powder. *J. Environ. Chem. Eng.* **2021**, *9* (1), No. 104655.

(22) Florea, L.; Hennart, A.; Diamond, D.; Benito-Lopez, F. Synthesis and Characterisation of Spiropyran-Polymer Brushes in Micro-Capillaries: Towards an Integrated Optical Sensor for Continuous Flow Analysis. *Sens. Actuators B Chem.* **2012**, *175*, 92−99.

(23) Burns, C. T.; Choi, S. Y.; Dietz, M. L.; Firestone, M. A. Acidichromic Spiropyran-Functionalized Mesoporous Silica: Towards

Stimuli-Responsive Metal Ion Separations Media. *Sep. Sci. Technol.* **2008**, *43* (9−10), 2503−2519.
(24) Barachevsky, V. A. Photochromic Organo-Silica Nanoparticles. *Russ. J. Gen. Chem.* **2021**, *91* (9), 1875−1888.
(25) Rosario, R.; Gust, D.; Hayes, M.; Jahnke, F.; Springer, J.; Garcia, A. A. Photon-Modulated Wettability Changes on Spiropyran-Coated Surfaces. *Langmuir* **2002**, *18* (21), 8062−8069.
(26) Bohaty, A. K.; Newton, M. R.; Zharov, I. Light-Controlled Ion Transport through Spiropyran-Modified Nanoporous Silica Colloidal Films. *J. Porous Mater.* **2010**, *17* (4), 465−473.
(27) Ueda, M.; Kim, H.-B.; Ichimura, K. Photocontrolled Aggregation of Colloidal Silica. *J. MATER CHEM* **1994**, *4*, 883.
(28) He, Y.; Shao, L.; Usman, I.; Hu, Y.; Pan, A.; Liang, S.; Xu, H. A Ph-Responsive Dissociable Mesoporous Silica-Based Nanoplatform Enabling Efficient Dual-Drug Co-Delivery and Rapid Clearance for Cancer Therapy. *Biomater. Sci.* **2020**, *8* (12), 3418−3429.
(29) Piech, M.; George, M. C.; Bell, N. S.; Braun, P. V. Patterned Colloid Assembly by Grafted Photochromic Polymer Layers. *Langmuir* **2006**, *22* (4), 1379−1382.
(30) Kinashi, K.; Nakamura, S.; Ono, Y.; Ishida, K.; Ueda, Y. Reverse Photochromism of Spiropyran in Silica. *J. Photochem. Photobiol. Chem.* **2010**, *213* (2−3), 136−140.
(31) Okabe, Y.; Ogawa, M. Photoinduced Adsorption of Spiropyran into Mesoporous Silicas as Photomerocyanine. *RSC Adv.* **2015**, *5* (123), 101789−101793.
(32) Yang, Y.; Zhao, H.; Li, Y.; Chen, Y.; Wang, Z.; Wu, W.; Hu, L.; Zhu, J. Tuning the Photochromism of Spiropyran in Functionalized Nanoporous Silica Nanoparticles for Dynamic Anticounterfeiting Applications. *ACS Omega* **2023**, *8* (18), 16459−16470.
(33) Grady, M. E.; Birrenkott, C. M.; May, P. A.; White, S. R.; Moore, J. S.; Sottos, N. R. Localization of Spiropyran Activation. *Langmuir* **2020**, *36* (21), 5847−5854.
(34) He, Y.; Fan, X.; Wu, X.; Hu, T.; Zhou, F.; Tan, S.; Chen, B.; Pan, A.; Liang, S.; Xu, H. Ph-Responsive Size-Shrinkable Mesoporous Silica-Based Nanocarriers for Improving Tumor Penetration and Therapeutic Efficacy. *Nanoscale* **2022**, *14* (4), 1271−1284.
(35) Alam, A. U.; Howlader, M. M. R.; Deen, M. J. The Effects of Oxygen Plasma and Humidity on Surface Roughness, Water Contact Angle and Hardness of Silicon, Silicon Dioxide and Glass. *J. Micromechanics Microengineering* **2014**, *24* (3), No. 035010.
(36) Gómez, J. E.; Sandoval, J. E. The Effect of Conditioning of Fused-silica Capillaries on Their Electrophoretic Performance. *ELECTROPHORESIS* **2008**, *29* (2), 381−392.
(37) Sun, P.; Liu, G.; Lv, D.; Dong, X.; Wu, J.; Wang, D. Effective Activation of Halloysite Nanotubes by Piranha Solution for Amine Modification via Silane Coupling Chemistry. *RSC Adv.* **2015**, *5* (65), 52916−52925.
(38) Acres, R. G.; Ellis, A. V.; Alvino, J.; Lenahan, C. E.; Khodakov, D. A.; Metha, G. F.; Andersson, G. G. Molecular Structure of 3-Aminopropyltriethoxysilane Layers Formed on Silanol-Terminated Silicon Surfaces. *J. Phys. Chem. C* **2012**, *116* (10), 6289−6297.
(39) Sypabekova, M.; Hagemann, A.; Rho, D.; Kim, S. Review: 3-Aminopropyltriethoxysilane (APTES) Deposition Methods on Oxide Surfaces in Solution and Vapor Phases for Biosensing Applications. *Biosensors* **2023**, *13* (1), 36.
(40) Zhuravlev, L. T. Concentration of Hydroxyl Groups on the Surface of Amorphous Silicas. *Langmuir* **1987**, *3* (3), 316−318.
(41) Madeley, J. D.; Richmond, R. C. A Procedure for Determining the Concentration of Hydroxyl Groups on Silica Surfaces. *Z. Für Anorg. Allg. Chem.* **1972**, *389* (1), 92−96.
(42) Rösch, U.; Yao, S.; Wortmann, R.; Würthner, F. Fluorescent H-Aggregates of Merocyanine Dyes. *Angew. Chem.* **2006**, *118* (42), 7184−7188.
(43) Ikbal, M.; Balogh, D.; Mervinetsky, E.; Sfez, R.; Yitzchaik, S. Light-Induced Aggregation of Gold Nanoparticles and Photoswitching of Silicon Surface Potential. *J. Phys. Chem. C* **2017**, *121* (48), 27176−27181.


https://doi.org/10.1021/acsomega.4c01607
*ACS Omega* 2024, 9, 29401−29409